

Instrumented anvil-on-rod tests for constitutive model validation and determination of strain-rate sensitivity of ultrafine-grained copper

M. Martin^a, A. Mishra^b, M.A. Meyers^b, N.N. Thadhani^{a,*}

^a School of Materials Science and Engineering, Georgia Institute of Technology, Atlanta, GA 30332, United States

^b Department of Mechanical and Aerospace Engineering, University of California, San Diego, CA 92093, United States

Received 8 December 2006; received in revised form 28 January 2007; accepted 31 January 2007

Abstract

Anvil-on-rod impact tests were performed on as-received (cold-rolled) OFHC copper rods and copper processed by 2- or 8-passes of equal channel angular pressing (ECAP). The average grain size ranged from $\sim 30\ \mu\text{m}$ for the as-received sample to $\sim 440\ \text{nm}$ for the 8-pass sample. The dynamic deformation states of the samples were captured by high-speed digital photography and velocity interferometry was used to record the sample back (free) surface velocity. Computer simulations utilizing AUTODYN-2D hydrocode with the Johnson–Cook constitutive model were used to generate free surface velocity traces and transient deformation profiles for comparison with the experimental data. The comparison of experimental results with AUTODYN simulations provided a means for extracting the strain-rate sensitivity of copper as a function of grain size. Strain-rate sensitivity was found to increase as grain size decreased.

© 2007 Elsevier B.V. All rights reserved.

Keywords: Strain rate sensitivity; Grain size effects; Dynamic deformation; Ultrafine-grained (UFG) copper

1. Introduction

Nanocrystalline and ultrafine-grained (UFG) metals have unique mechanical properties (e.g., strength, hardness, and fatigue resistance) that render them good candidates for various structural applications [1–6]. Recent results indicate that strain-rate sensitivity in UFG metals is enhanced in comparison with conventional polycrystalline metals having micro-scale grains [7–12]. The strain-rate sensitivity of UFG copper has been studied by Gray et al. [13] by performing quasistatic compression tests and split Hopkinson pressure bar experiments on ECAP-processed specimens. This study revealed that the strain-rate sensitivity of UFG Cu is significantly higher than that of typical annealed, polycrystalline Cu, and its yield strength is above that extrapolated from the Hall–Petch relation. The work described in this paper is an extension of what has been previously done to determine the strain-rate sensitivity enhancement in UFG, ECAP-processed Cu at strain rates on the order of 10^3 to $10^5\ \text{s}^{-1}$ using dynamic reverse Taylor [14] anvil-on-rod impact tests.

The rod-on-rigid-anvil impact experiment developed by Taylor [14] in 1948 has become a standard method for investigating the high strain rate ($\sim 10^3$ to $10^5\ \text{s}^{-1}$) response of materials. In Taylor's impact experiment, a cylindrical specimen is accelerated to impact a rigid anvil and deformation propagates through the cylinder as a wave. After impact, the specimen is recovered and the changes in its dimensions are used to infer its dynamic flow strength [14,15]. This test has become a common tool for investigating the constitutive response of materials by attempting to reproduce the final deformed shape of the specimen with a constitutive model [15–19]. However, simply matching the final shape of the specimen does not necessarily provide a robust validation of the constitutive model since the deformation path is not considered [20].

Constitutive models based on empirical relationships (i.e., Johnson–Cook [16]) as well as physically based relationships (i.e., Zerilli–Armstrong [17]) have been commonly used in the past for comparison with experimental results. It is not the intent of this paper to choose one model or type of model over another, but simply to explain the validation method which was used in this study.

In recent years, the Taylor impact test has been performed in its reverse configuration, with the rigid anvil impacting a stationary rod-shaped sample, allowing for simultaneous

* Corresponding author. Tel.: +1 404 894 2651.

E-mail address: naresh.thadhani@mse.gatech.edu (N.N. Thadhani).

velocity interferometry of the free (back) surface velocity [21,22] and high-speed photography of the impact and specimen deformation throughout the entire deformation event. The implementation of multiple time-resolved diagnostics which monitor the entire deformation event allows for development of constitutive models and more robust validation, as described in detail by Eakins and Thadhani [20].

In the present work, a reverse Taylor anvil-on-rod impact test instrumented with high-speed digital photography and VISAR [23] velocity interferometry was used to investigate the dynamic deformation response of copper of nano- to micro-meter scale grain size. This method has also been applied to other materials including bulk metallic glass matrix composites [24].

Although it is useful to validate the extent to which a constitutive equation predicts the dynamic deformation response of a material by comparing simulations and experimental data, the method also enables determination of the constants which provide the best fit to the experimental data. In this study on Cu,

a well-characterized material, the Johnson–Cook equation [16], for which all relevant constants except for the strain-rate sensitivity were previously known [16] or determined experimentally, was used to extract the effect of grain size on strain rate sensitivity by examining three Cu specimens which had been processed using 0, 2, or 8 ECAP passes.

2. Experimental procedure

2.1. Materials

Commercially obtained OFHC, cold-rolled Cu was processed using a horizontal split ECAP die with an interior channel angle of 102° and exterior angle of 20° [25]. The processing route utilized was B_C , in which the sample is rotated by 90° in the same direction between consecutive passes [26,27]. Fig. 1 shows micrographs and grain size distributions of the as-received, 2-pass and 8-pass ECAP Cu. These figures show the reduction in

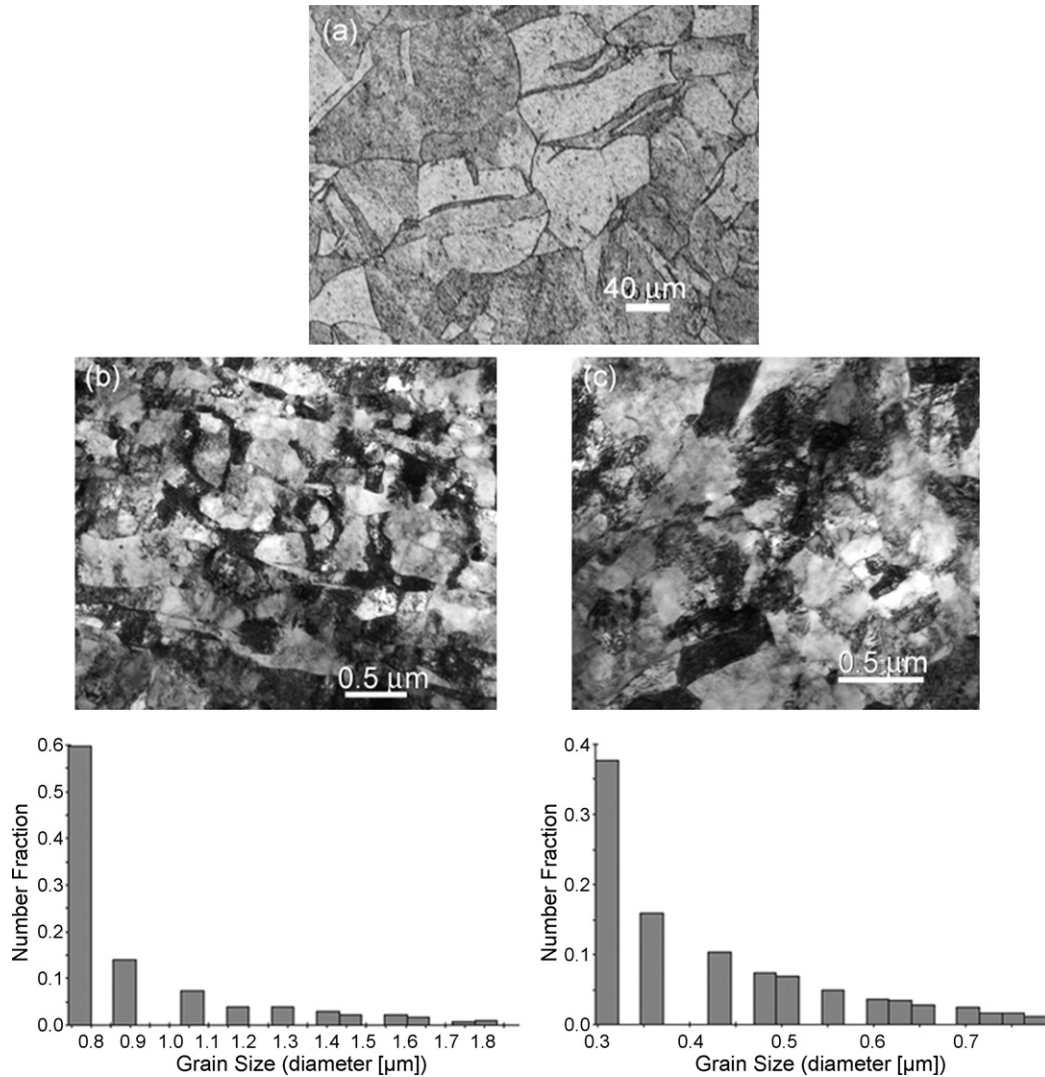


Fig. 1. (a) Optical micrograph of initial Cu with a grain size of $30\ \mu\text{m}$, and TEM micrographs of (b) 2-pass ECAP-processed Cu with a grain size of $\sim 890\ \text{nm}$, and (c) 8-pass ECAP-processed Cu with a grain size of $\sim 440\ \text{nm}$. The grain size distributions of the 2- and 8-pass ECAP samples are below the corresponding micrograph. The initial as-received Cu illustrates an extensive deformation cell substructure typical of cold-rolled rods, and the ECAP Cu shows clear evidence of refined grain size.

grain size that occurred with increasing ECAP passes. The as-received Cu had an average grain size, measured using the line intercept method on optical micrographs, of $\sim 30 \mu\text{m}$. After two ECAP passes the grain size had been reduced to an average size of $\sim 890 \text{ nm}$, with even further reduction to $\sim 440 \text{ nm}$ after eight ECAP passes.

The Cu samples were machined into cylindrical specimens of 4 mm diameter and 4 mm length for static testing and rods of 9.4 mm diameter and 40.13 mm length for dynamic testing. The rods were lapped on both ends with $45 \mu\text{m}$ diamond suspension to insure parallel surfaces.

2.2. Static compression testing

Compression tests were performed on the as-received (cold-rolled), 2-pass and 8-pass Cu samples. The tests were performed at strain rates of 5×10^{-3} and 1 s^{-1} using a Satec compression testing machine. These data were used to compare the strengths of the three differently processed specimens at various strain rates. The data collected at 1 s^{-1} were also used to determine the values of constants needed for modeling with the Johnson–Cook [16] equation, as described later.

2.3. Reverse Taylor impact tests

Instrumented reverse Taylor anvil-on-rod impact tests [20,24,28], were conducted to permit correlation of simulated deformation profiles with transient deformation states recorded during the experiment. A schematic of the reverse Taylor anvil-on-rod impact test setup is shown in Fig. 2. Complete experimental details are described in Ref. [20]. The projectile consisted of an 80 mm diameter 2024 Al sabot with a maraging steel rigid anvil plate ($\sim 6.2 \text{ mm}$ thickness) secured to the front surface. The rod-shaped samples were mounted onto a target ring and aligned with a laser beam to ensure parallel impact. An IMACON-200 high-speed digital camera, used to capture images of the deformation of the rods during impact, was triggered using crush pins. The free surface velocity of the back surface of the rod was captured in each experiment by a VISAR [23] probe, which was positioned behind the sample, as seen in Fig. 2. The details of each experiment, including the number of ECAP passes the specimen had undergone, the impact velocity, and average strain rate are given in Table 1. The average strain rate was defined based on the impact velocity and change in length of the specimen [29]. Higher strain rates (on the order of

Table 1

Experiment details including the number of ECAP passes the specimen had undergone during processing and the impact velocity

Material (no. of ECAP passes)	Impact velocity (m/s)	Average strain rate (s^{-1})
As-received (cold-rolled)	88	1093
2	123	1528
8	125	1557

The average strain rate was estimated using the impact velocity and change in length of the specimen according to the method described by Meyers [29].

3600 s^{-1} for 125 m/s impact of the 8-pass sample) were experienced by the specimens during the early stages of impact, and the strain rate subsequently decreased as deformation continued.

2.4. Autodyn-2D modeling

AUTODYN simulations of the anvil-on-rod impact experiments were performed to validate the constitutive response of the ECAP Cu specimens using the Johnson–Cook constitutive equation [16].

$$\sigma = [A + B\epsilon^n][1 + C \ln \dot{\epsilon}^*][1 - T^{*m}] \quad (1)$$

The unknown strain rate sensitivity constant, C , was generated by fitting the simulated free surface velocity trace to that determined experimentally using VISAR. The models were further validated by comparing simulated transient deformation profiles with the images captured during deformation. Simulations were run in 2D as an axisymmetric problem, and gauges were placed on the specimen's rear surface to track the free surface velocity; the model setup can be seen in Fig. 3.

For the Johnson–Cook equation, the hardening constant, B , and hardening exponent, n , were obtained from stress–strain data measured at $\dot{\epsilon} = 1 \text{ s}^{-1}$. The yield strength coefficient, A , was left at 90 MPa, the value determined by Johnson and Cook [16] since this value represents yield stress in undeformed copper. The thermal softening exponent, m , was also left as determined by Johnson and Cook. The strain rate constant, C , the only remaining variable, was then empirically obtained by fitting the simulated free surface velocity trace with that obtained experimentally, as described by Eakins and Thadhani [20].

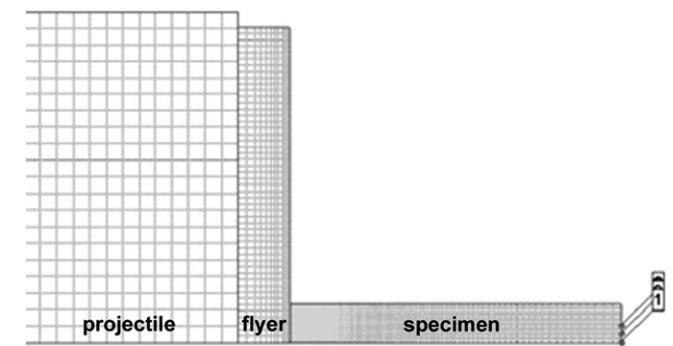


Fig. 3. Axisymmetric problem setup and mesh in AUTODYN-2D showing the projectile (partial), flyer plate and specimen. The gauge on the back (free) surface of the specimen tracks the free surface velocity.

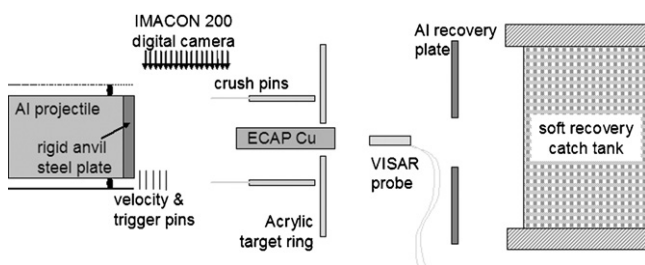


Fig. 2. Schematic of the reverse Taylor anvil-on-rod impact test setup.

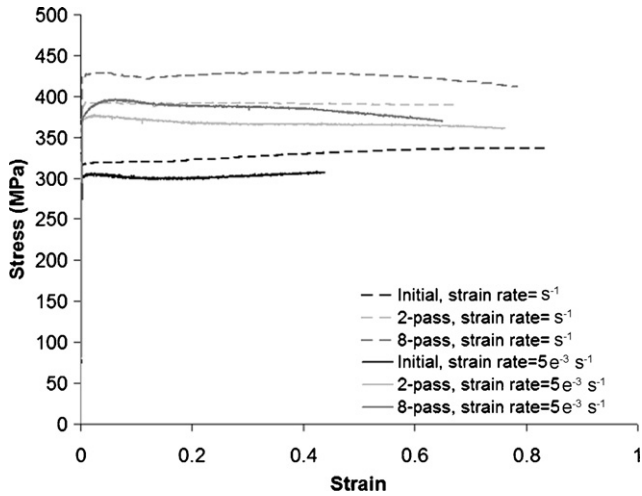


Fig. 4. True stress–strain plots for Cu samples in as-received state and after two and eight ECAP passes ($\dot{\epsilon} = 5 \times 10^{-3}$ and 1 s^{-1}).

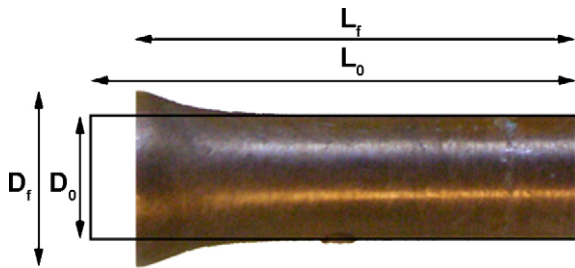


Fig. 5. Eight-pass Cu specimen recovered after reverse Taylor anvil-on-rod impact tests at 125 m/s.

3. Results and discussion

3.1. Static compression testing

Static stress–strain curves were obtained for the as-received, 2- and 8-pass ECAP Cu specimens. Fig. 4 shows the true stress–strain response for as-received, 2- and 8-pass ECAP Cu at strain rates of 5×10^{-3} and 1 s^{-1} . The effects of significant deforma-

Table 2

Quasistatic 0.2% offset flow stress values for ECAP specimens tested in compression at two different (quasi-static) strain rates

No. of ECAP passes	Flow stress at $\dot{\epsilon} = 5 \times 10^{-3} \text{ s}^{-1}$ (MPa)	Flow stress at $\dot{\epsilon} = 1 \text{ s}^{-1}$ (MPa)
0	301	316
2	371	388
8	374	421

Table 3

Final axial and areal strain values measured from recovered specimens

No. of ECAP passes	Impact velocity (m/s)	Axial strain, $\epsilon = \ln(L_f/L_0)$	Areal strain, $\epsilon = 1 - (A_0/A)$
0	88	0.137	0.377
2	123	0.177	0.549
8	125	0.169	0.518

tion during ECAP processing and the accompanying reduction in grain size on the strength of these copper specimens were evident in the static test data. It is important to note that even the as-received (0-pass) Cu sample had an extensive deformation substructure due to cold-rolling consistent with the almost zero work hardening observed in the stress–strain curves shown in Fig. 4. Table 2 lists the values of the flow strengths obtained from quasistatic experiments. For both static strain rates, these results show an increase in flow strength with increasing ECAP passes.

3.2. Dynamic testing

Reverse Taylor anvil-on-rod impact experiments were performed on the as-received Cu specimen at 88 m/s, the 2-pass ECAP Cu specimen at 123 m/s, and the 8-pass ECAP Cu specimen at 125 m/s. A representative image of the recovered 8-pass specimen (impacted at 125 m/s) is shown in Fig. 5, with indications of its initial and final dimensions. Table 3 lists the final axial and areal strains measured from the recovered samples. Compar-

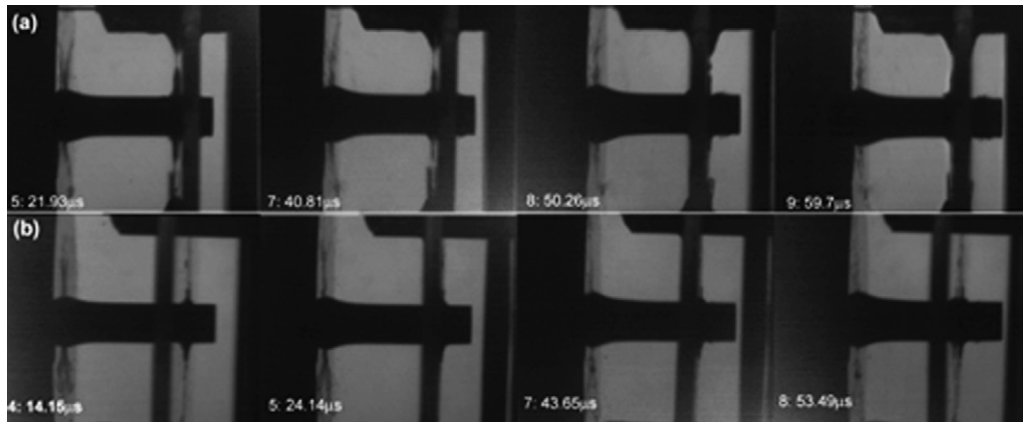


Fig. 6. Four of 16 high-speed digital images from (a) impact of a 2-pass ECAP Cu specimen at 123 m/s and (b) impact of an 8-pass ECAP Cu specimen at 125 m/s. These images show the projectile + flyer plate assembly accelerating from the left to impact the stationary rod-shaped specimen, which deforms by mushrooming of the impact face and decrease in specimen length. Comparison of the 2- and 8-pass specimens shows that the 2-pass specimen is deforming more than the 8-pass specimen.

ison of the recovered ECAP specimens showed that the 8-pass specimen exhibited less deformation than the 2-pass specimen during dynamic testing at a similar impact velocity, due to greater strain hardening achieved during additional ECAP passes.

Fig. 6 shows 4 of 16 images captured during reverse Taylor anvil-on-rod testing of the (a) 2- and (b) 8-pass ECAP Cu specimens. These images show the projectile + flyer plate assembly accelerating from the left to impact the stationary rod-shaped specimen, which is in the center of the image. It can be seen in these images that the impact face of the specimens are expanding, or mushrooming, and the length is decreasing. Comparison of the 2- and 8-pass specimens shows that the 2-pass specimen is deforming more than the 8-pass specimen due to the additional strain hardening endured by the 8-pass specimen during six more ECAP passes.

3.3. AUTODYN-2D modeling

AUTODYN simulations were performed using the Johnson–Cook constitutive model with hardening constants obtained from stress-strain data measured at strain rate of 1 s^{-1} and an empirically determined strain-rate sensitivity parameter that was modified such that the simulated free surface velocity trace matched the experimentally measured velocity trace. Fig. 7 shows the comparisons between the experimentally measured free surface velocity traces and those obtained from the AUTODYN simulation using the Johnson–Cook model for each specimen. It can be seen that the simulations capture details of the slope and peak of the free surface velocity and result in a very close fit to the experimental data. The differences between the simulation and experiment in the first step size appear to be more obvious in the case of the 8-pass ECAP sample than the others. We attribute this to the effects of the ultrafine grains and their associated boundaries, the details of which are not captured in the simulations. The increase in the number of grains with increasing grain size can result in more dispersion of the elastic waves, and consequently lower amplitude reverberation, which was observed in the experimental traces, as compared to the simulated traces.

The final values of the Johnson–Cook constants used for each case resulting in the best match to the experimental data are summarized in Table 4. The Johnson–Cook equation with the modified constants was then used to generate deformation profiles for comparison with deformation profiles of the final recovered samples, as well as the transient profiles recorded with the high-speed digital camera. The dimensions of each of the recovered specimens and those from the final state of the simulation are reported in Table 5. The simulations show final deformation geometries that differ from experimental values by $<7.38\%$ in length and $<2.01\%$ in impact face radius for each sample. The larger error in the final length is due to the physical measurements performed on the recovered specimens, which had slightly non-parallel ends and non-round impact face due to secondary impact in catch tank.

The experimental and simulated length and impact face radius at transient times are compared in Tables 6 and 7 for the 2-pass and 8-pass samples, respectively. These results demonstrate a

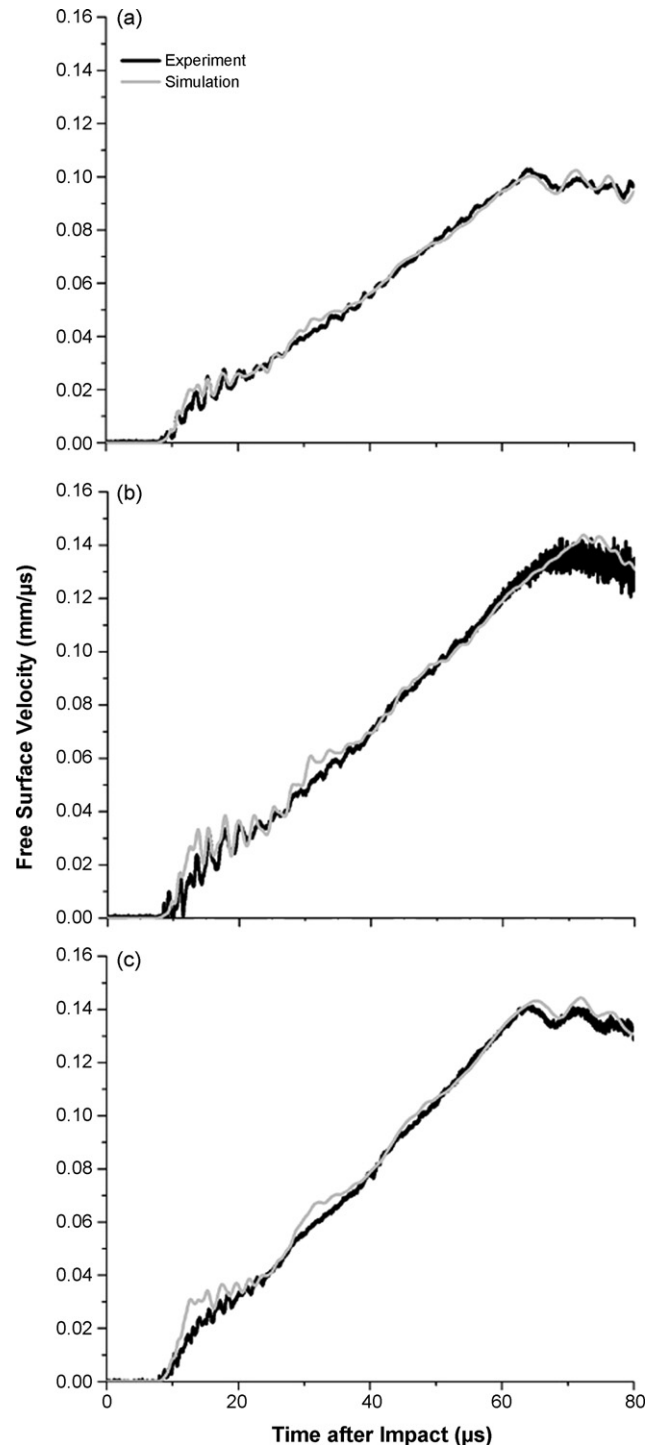


Fig. 7. Simulated vs. experimental free surface velocity trace for each ECAP Cu specimen. Simulation is based on modified Johnson–Cook parameters from stress-strain data and empirical fit to the experimental free surface velocity trace. (a) Initial Cu, 88 m/s, (b) 2-pass Cu, 123 m/s, and (c) 8-pass Cu, 125 m/s.

close match ($<2.7\%$ difference for each time) of these dimensions between simulations and experiments for each of the transient times, indicating that the model provides an accurate prediction of the deformation, and the constants obtained can be used to further investigate the deformation response. Comparisons of the simulated and experimental transient profiles of

Table 4
Modified Johnson–Cook parameters used in AUTODYN simulations

No. of ECAP passes	Yield stress, A (MPa)	Hardening constant, B (MPa)	Hardening exponent, n	Strain rate constant, C	Thermal softening exponent, m
0	90	340	0.0334	0.009	1.09
2	90	390	0	0.011	1.09
8	90	423	0	0.017	1.09

A and m were left as determined by Johnson and Cook [16], B and n were determined using $\sigma = B\varepsilon^n$ in the plastic range of the stress–strain data obtained at $\dot{\varepsilon} = 1 \text{ s}^{-1}$, and C was then determined by empirically fitting the simulations to the experimental data.

Table 5
Comparison of final dimensions from simulations and experiments

No. of ECAP passes	L_f (mm)	%Difference	R_f at impact face (mm)	%Difference
0	Expt: 35.00 Sim: 37.53	7.23	Expt: 5.97 Sim: 6.09	2.01
2	Expt: 33.63 Sim: 36.17	7.03	Expt: 6.96 Sim: 7.03	1.01
8	Expt: 33.88 Sim: 36.38	7.38	Expt: 6.73 Sim: 6.86	1.93

Experimental values were measured from recovered specimens, which had undergone secondary impact in the catch tank, resulting in non-parallel ends or imperfectly round cross sections, and subsequently a small amount of error associated with measurement of these values, so average values are reported.

Table 6
Transient dimensions of the 2-pass ECAP specimen during deformation obtained from high-speed digital images during the experiment and from simulations at corresponding times

Time (μs)	L (Expt) (mm)	L (Sim) (mm)	%Difference in length	R (Expt) (mm)	R (Sim) (mm)	%Difference in radius
12.49	38.67 ± 0.09	38.69	0.06	5.93 ± 0.08	5.75	1.55
21.93	37.80 ± 0.11	37.82	0.04	6.28 ± 0.18	6.29	0.06
31.37	36.94 ± 0.17	37.10	0.43	6.59 ± 0.14	6.65	0.43
40.81	36.37 ± 0.10	36.53	0.43	6.91 ± 0.23	6.91	0.00
50.26	36.16 ± 0.10	36.19	0.07	6.83 ± 0.43	7.02	1.41

Table 7
Transient dimensions of the 8-pass ECAP specimen during deformation obtained from high-speed digital images during the experiment and from simulations at corresponding times

Time (μs)	L (Expt) (mm)	L (Sim) (mm)	%Difference in length	R (Expt) (mm)	R (Sim) (mm)	%Difference in radius
14.15	38.28 ± 0.06	38.53	0.66	6.06 ± 0.14	5.81	2.03
24.14	37.51 ± 0.20	37.63	0.31	6.40 ± 0.17	6.33	0.52
33.82	36.43 ± 0.06	36.99	1.55	6.72 ± 0.27	6.64	0.57
43.65	36.44 ± 0.28	36.50	0.15	6.66 ± 0.22	6.82	1.19
53.49	36.44 ± 0.03	36.31	0.37	6.52 ± 0.19	6.87	2.70

the 2- and 8-pass ECAP Cu specimens at selected times during impact are shown in Fig. 8. A close correlation, within the pixel uncertainty associated with the image resolution, between the simulated and experimental deformation states is observed. The correlation provides further validation that the Johnson–Cook model is accurately describing deformation of the as-received (cold-rolled) and ECAP Cu, so the significance of each constant can be further evaluated.

Values of the dynamic flow stress were calculated using the Johnson–Cook equation, and are listed in Table 8. The variation of flow strength as a function of strain rate for each specimen is plotted in Fig. 9. It can be seen from this plot that the 8-pass ECAP sample is consistently stronger than the 2-pass and as-

received Cu samples. The plot of flow strengths also indicates the effect of strain rate on the flow strength, with a $\sim 42\%$ increase in strength of the as-received Cu versus a $\sim 53\%$ increase for the 8-pass ECAP Cu over strain rates of seven orders of magnitude.

Table 8
Dynamic flow stress values calculated using the Johnson–Cook equation

No. of ECAP passes	Dynamic flow stress, Johnson–Cook (Eq. (1)) (MPa)
0	427
2	513
8	571

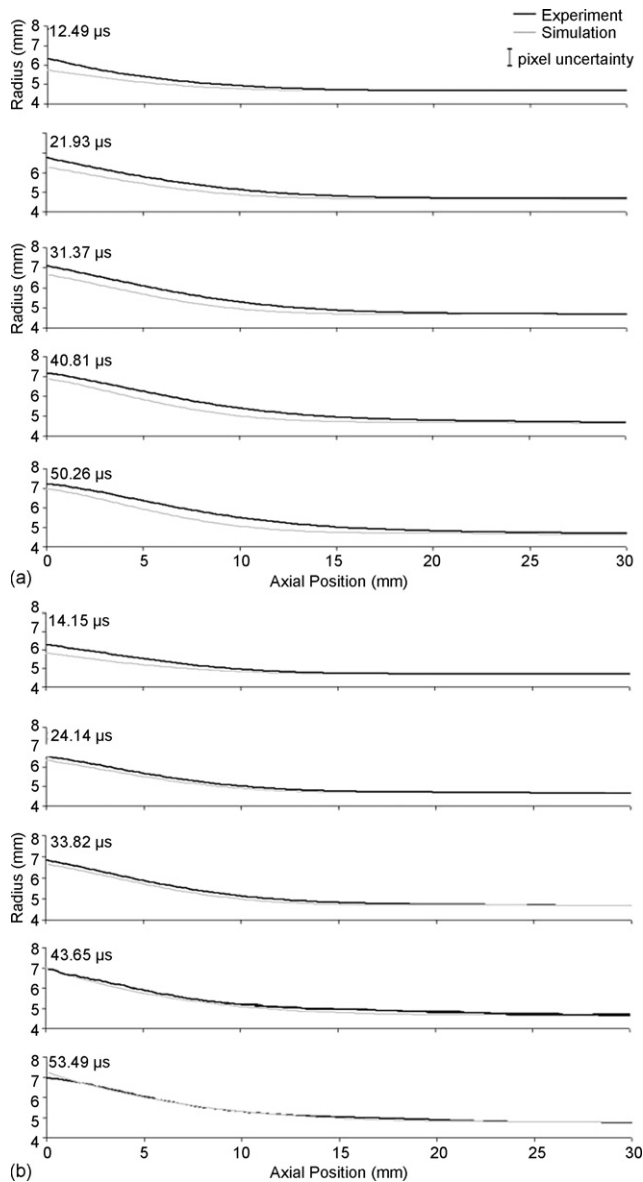


Fig. 8. Radius as a function of distance from impact end plots comparing Johnson–Cook simulations with the experimental transient deformation profiles at various times after impact of the (a) 2- and (b) 8-pass ECAP Cu samples impacted at 123 and 125 m/s, respectively. (a) shows a marker indicating the maximum pixel uncertainty corresponding to the image resolution.

Table 4 lists a strain rate constant of 0.009 for the as-received Cu, 0.011 for 2-pass ECAP Cu, and 0.017 for the 8-pass ECAP Cu, which are the strain rate constants that provided the best fit of the simulation to the experimental free surface velocity trace and transient profiles. These values show an increase in strain-rate sensitivity of the ECAP samples, which is due to the effect of ultrafine grain size, consistent with that observed in other studies [9,13]. The strain rate sensitivity of the as-received Cu is comparable with that for microcrystalline fcc materials including Cu as determined by Conrad [30] (Conrad found a strain rate sensitivity of 0.004.). The 2-pass ECAP specimen shows only a slight increase in strain rate sensitivity compared to the initial sample, possibly due to incomplete formation of sub-grain structure. In contrast, the 8-pass ECAP sample, with a ~ 440 nm grain size,

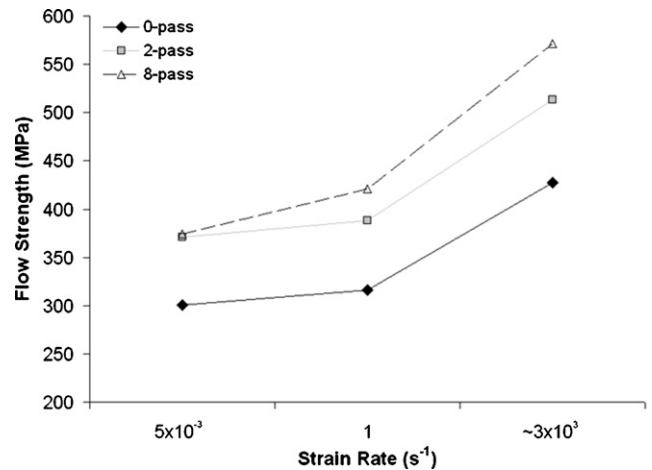


Fig. 9. Flow strengths of the ECAP Cu specimens at different strain rates ranging seven orders of magnitude.

exhibited nearly twice as much strain-rate sensitivity as the as-received Cu. These results are consistent with the mechanism explained by Goeken et al. [8], who have observed an enhanced strain rate sensitivity corresponding to a decrease in activation volume $V = (\sqrt{3}kT/\sigma m)$, which has been attributed to a change in the rate-controlling mechanism from forest dislocations to other behaviors in the ultrafine grain size domain.

4. Conclusions

The dynamic deformation of as-received (cold-rolled) and subsequently ECAP-processed Cu tested using reverse Taylor anvil-on-rod impact experiments was captured by high speed digital photography and compared with AUTODYN-2D simulations using the Johnson–Cook constitutive equation with constants obtained from stress–strain data and by fitting to an experimentally measured free surface velocity trace. The constitutive equation provided a good fit to the final shape of each of the impacted specimens, as well as the transient deformation shapes. The constitutive equation also enabled the evaluation of the strain-rate sensitivity parameter, which was determined to be 0.009 for the as-received Cu, 0.011 for 2-pass ECAP Cu, and 0.017 for 8-pass ECAP Cu. These results show an increase in strain-rate sensitivity with decreasing grain size, consistent with previous observations [9,13].

Acknowledgements

Research at Georgia Tech was supported by ARO Grant no. E-48148-MS-000-05123-1 (Dr. Mullins program monitor), a Boeing Graduate Fellowship, and a NASA Jenkins Fellowship. Research at UCSD was supported by the National Science Foundation under Grant CMS-0210173 (NIRT).

References

- [1] C. Suryanarayana, Int. Mater. Rev. 40 (1995) 41–64.
- [2] R.Z. Valiev, N.A. Krasilnikov, N.K. Tsenev, Mater. Sci. Eng. A 137 (1991) 35–40.

- [3] R.Z. Valiev, A.V. Korznikov, R.R. Mulyukov, *Mater. Sci. Eng. A* 168 (1993) 141–148.
- [4] R.Z. Valiev, E.V. Kozlov, Y.F. Ivanov, J. Lian, A.A. Nazarov, B. Baudelet, *Acta Metall. Mater.* 42 (1994) 2467–2475.
- [5] V.Y. Gertsman, R. Birringer, R.Z. Valiev, H. Gleiter, *Scripta Mater.* 30 (1994) 229–234.
- [6] J.R. Weertman, *Mater. Sci. Eng. A* 166 (1993) 161–167.
- [7] L. Lu, S.X. Li, K. Lu, *Scripta Mater.* 45 (2001) 1163–1169.
- [8] J. May, H.W. Hoppel, M. Goeken, in: Z. Horita, T.G. Langdon (Eds.), *Proceedings of the 3rd International Conference of Nanomaterials by Severe Plastic Deformation. Nanospd 3/3rd International Conference of Nanomaterials by Severe Plastic Deformation, Nanospd 3, Japan, 2005.*
- [9] Q. Wei, S. Cheng, K.T. Ramesh, E. Ma, *Mater. Sci. Eng. A* 381 (2004) 71.
- [10] R. Schwaiger, B. Moser, M. Dao, N. Chollacoop, S. Suresh, *Acta Mater.* 51 (2003) 5159–5172.
- [11] F. Dalla Torre, H. Van Swygenhoven, M. Victoria, *Acta Mater.* 50 (2002) 3957–3970.
- [12] Y.M. Wang, E. Ma, *Mater. Sci. Eng. A* 375–377 (2004) 46–52.
- [13] G.T. Gray, T.C. Lowe, C.M. Cady, R.Z. Valiev, I.V. Aleksandrov, *Nanostruct. Mater.* 9 (1997) 477.
- [14] G. Taylor, *Proc. R. Soc. London A* 194 (1948) 289–299.
- [15] M.L. Wilkins, M.W. Guinan, *J. Appl. Phys.* 44 (1973) 1200–1206.
- [16] G.R. Johnson, W.H. Cook, *Proceedings of the 7th International Symposium on Ballistics, The Hague, The Netherlands, 1983, p. 541.*
- [17] F.J. Zerilli, R.W. Armstrong, *J. Appl. Phys.* 61 (1987).
- [18] J.B. Hawkyard, *Int. J. Mech. Sci.* 11 (1969) 313–333.
- [19] W.H. Gust, *J. Appl. Phys.* 53 (1982) 3566–3575.
- [20] D. Eakins, N.N. Thadhani, *J. Appl. Phys.* 100 (2006), 073503–073501–073508.
- [21] I. Rohr, H. Nahme, K. Thoma, *Int. J. Impact Eng.* 31 (2005) 401–433.
- [22] I. Rohr, H. Nahme, K. Thoma, *J. Phys. IV* 110 (2003) 513–518.
- [23] L.M. Barker, R.E. Hollenbach, *J. Appl. Phys.* 43 (1972) 4669–4675.
- [24] M. Martin, N.N. Thadhani, L. Kecskes, R. Dowding, *Scripta Mater.* 55 (2006) 1019–1022.
- [25] A. Mishra, V. Richard, F. Gregori, R.J. Asaro, M.A. Meyers, *Mater. Sci. Eng. A* (2005) 410–411.
- [26] V.M. Segal, *Mater. Sci. Eng. A* 197 (1995) 157–164.
- [27] S. Ferrasse, V.M. Segal, K.E. Hartwig, R.E. Goforth, *Metal. Mater. Trans.* 28A (1997) 1047–1057.
- [28] M. Martin, S. Hanagud, N.N. Thadhani, *Mater. Sci. Eng. A* 443 (2007) 209–218.
- [29] M.A. Meyers, *Dynamic Behavior of Materials*, Wiley-Interscience, New York, 1994, p. 668.
- [30] H. Conrad, in: V. F. Zackey (Ed.) *High Strength Materials*, 1965.